MULTIGAIN-STAGE InGaAs AVALANCHE PHOTODIODE WITH ENHANCED GAIN AND REDUCED EXCESS NOISE

George M. Williams, Madison Compton, and Andrew S. Huntington, Allegro MicroSystems
David A. Ramirez, Majeed M. Hayat, Center for High Technology Materials, University of New Mexico

ABSTRACT

The design, fabrication, and test of an InGaAs avalanche photodiode (APD) for 950–1650 nm wavelength sensing applications are reported. The APD is grown by molecular beam epitaxy on InP substrates from lattice-matched InGaAs and InAlAs alloys. Avalanche multiplication inside the APD occurs in a series of asymmetric gain stages whose layer ordering acts to enhance the rate of electron-initiated impact ionization and to suppress the rate of hole-initiated ionization when operated at low gain. The multiplication stages are cascaded in series, interposed with carrier relaxation layers in which the electric field is low, preventing avalanche feedback between stages. These measures result in much lower excess multiplication noise–and stable linear-mode operation at much higher avalanche gain–than is characteristic of APDs fabricated from the same semiconductor alloys in bulk. The noise suppression mechanism is analyzed by simulations of impact-ionization spatial distribution and gain statistics, and measurements on APDs implementing the design are presented. The devices employing this design are demonstrated to operate at linear-mode gain in excess of 6,000 without avalanche breakdown. Excess noise characterized by an effective impact-ionization-rate ratio below 0.04 were measured at gains over 1,000.

INTRODUCTION

Linear-mode APDs are used in optical receivers for applications such as optical communications and lidar, which benefit from the internal photocurrent gain, fast response, compact size, durability, and low cost of the APD. The gain of a linear-mode APD improves the signal-to-noise ratio of a photoreceiver by boosting the signal photocurrent relative to circuit noise sources downstream in the signal chain.

The slope of an APD gain curve as a function of reverse bias limits the gain at which it can be used. The slope of the gain curve is a challenge for many applications because avalanche gain (M_{DC}) increases asymptotically in the vicinity of the breakdown voltage (V_{br}) of the APD, according to the empirical relation:

Equation 1:

$$M_{DC} = \left[1 - V/V_{br}\right]^{-n},$$

where the parameter n controls how quickly the avalanche gain rises as V approaches its vertical asymptote at V_{br}. This relation persists for all APDs in which both carrier types (electrons and holes) can initiate impact ionization. [1]

[1]   P. Bhattacharya, Semiconductor Optoelectronic Devices, 2nd ed., Upper Saddle River, NJ: Prentice Hall, 1997, p. 384.

Stable operation of APDs characterized by large values of n becomes impracticable at high gains because V/V_{br} cannot be adequately controlled.

Avalanche noise imposes a separate limit on the useable gain of an APD. In the limit of high avalanche gain, the sensitivity of a hypothetical photoreceiver that employs an ideal "noiseless" APD is limited by the shot noise on the optical signal itself. However, most APDs generate multiplication noise in excess of the shot noise already present on the optical signal; this excess multiplication noise intensifies with increasing avalanche gain, such that for any given level of downstream amplifier noise, there is a limit to how much avalanche gain is useful. If the avalanche gain increases beyond the optimal value, the shot noise will increase faster than the amplified signal photocurrent, which degrades the signal-to-noise ratio.

Excess multiplication noise results from the stochastic nature of the impact-ionization process that amplifies the primary photocurrent of an APD. For most linear-mode APDs, the gain distribution is that derived by McIntyre. [2] The McIntyre distribution is far from Gaussian for small inputs (i.e., for a small number of primary photocarriers injected into the multiplier), with a pronounced positive skew. For larger inputs, the McIntyre distribution approaches Gaussian due to the central limit theorem, and avalanche noise can be quantified for analysis with other common circuit noise sources by computing the variance of the gain. The Burgess variance theorem [3],[4] gives the variance of the multiplied output n for a primary carriers generated by a Poisson process and injected into a multiplier characterized by mean gain M_{DC} and random gain variable m [5]:

Equation 2:

$$var(n) = M_{DC}^2 var(a) + \langle a \rangle var(m) = M_{DC}^2 F \langle a \rangle,$$

where the excess noise factor, F, is defined as:

Equation 3:

$$F \equiv \langle m^2 \rangle / M_{DC}^2 \; .$$

For most linear-mode APDs, the excess noise factor has the gain dependence derived by McIntyre for uniform junctions [6]:

Equation 4:

$$F = M_{DC} \left[1 - (1-k) \left(\frac{(M_{DC} - 1)}{M_{DC}} \right)^2 \right] .$$

In Equation 4, the parameter k is the ratio of the hole-to-electron impact-ionization rates. When $k > 0$, k is the slope of the excess noise curve as a function of gain, in the limit of high gain. For single-carrier multiplication, $k = 0$, and $F \rightarrow 2$ in the limit of high gain. Another feature of single-carrier $k = 0$ multiplication is that avalanche breakdown cannot occur. Without participation of one carrier type, all impact-ionization chains must eventually self-terminate because all carriers of the type capable of initiating impact ionization soon exit the multiplying junction. The gain curve of a $k = 0$ APD does not exhibit the vertical asymptote described by Equation 1, which enables stable operation at higher gain than a $k > 0$ APD.

Important exceptions to the excess noise factor formula in Equation 4 include APDs in which the carrier dead space is a significant portion of the width of the multiplying junction, [7],[8],[9],[10] those in which a change in alloy composition modulates the impact-ionization threshold energy and rate across the multiplying

[2] R. J. McIntyre, "The Distribution of Gains in Uniformly Multiplying Avalanche Photodiodes: Theory," IEEE Trans. Electron. Devices, vol. ED-19, pp. 703–713, Jun. 1972.

[3] R. E. Burgess, "Homophase and heterophase fluctuations in semiconducting crystals," Discussions of the Faraday Society, vol. 28, pp. 151–158, 1959.

[4] R. E. Burgess, "Some topics in the fluctuations of photo-processes in solids," Journal of Physics and Chemistry of Solids, vol. 22, pp. 371–377, Dec. 1961.

[5] M. C. Teich, K. Matsuo, and B. E. A. Saleh, "Excess Noise Factors for Conventional and Superlattice Avalanche Photodiodes and Photomultiplier Tubes," IEEE J. Quantum Electron., vol. QE-22, pp. 1184-1193, Aug. 1986.

[6] R. J. McIntyre, "Multiplication noise in uniform avalanche diodes," IEEE Trans. Electron. Devices, vol. ED-13, pp. 164–168, Jan. 1966.

[7] K. A. Anselm, P. Yuan, C. Hu, C. Lenox, H. Nie, G. Kinsey, J. C. Campbell, and B. G. Streetman, "Characteristics of GaAs and AlGaAs homojunction avalanche photodiodes with thin multiplication regions," Appl. Phys. Lett., vol. 71, pp. 3883–3885, Dec. 1997.

[8] C. Lennox, P. Yuan, H. Nie, O. Bakelov, C. Hansing, J. C. Campbell, A. L. Holmes, Jr., and B. G. Streetman, "Thin multiplication region InAlAs homojunction avalanche photodiodes," Appl. Phys. Lett., vol. 73, pp. 783–784, Aug. 1998.

[9] M. A. Saleh, M. M. Hayat, B. E. A. Saleh, and M. C. Teich, "Dead-Space-Based Theory Correctly Predicts Excess Noise Factor for Thin GaAs and AlGaAs Avalanche Photodiodes," IEEE Trans. Electron. Devices, vol. 47, pp. 625–633, Mar. 2000.

[10] C. H. Tan, J. P. R. David, G. J. Rees, R. C. Tozer, and D. C. Herbert, "Treatment of soft threshold in impact ionization," J. Appl. Phys., vol. 90, pp. 2538–2543, Sep. 2001.

junction, [11],[12],[13],[14],[15],[16] and those made from semiconductor alloys with band structures that combine the traits of single-carrier-dominated multiplication ($k \sim 0$) with an abrupt carrier dead space, which results in correlations between the successive impact-ionization events. [17],[18],[19],[20],[21],[22] The cascaded multiplier design presented here applies similar physics to achieve high-gain operation with low excess multiplication noise.

REDUCING APD MULTIPLICATION NOISE

The goal of impact-ionization engineering (I²E) is to reduce excess multiplication noise by designing semiconductor structures in which certain impact-ionization chains that contribute to the gain distribution of a bulk multiplier have been eliminated, which narrows the gain distribution of the engineered multiplier. [23] In general, I²E designs use two tools: 1) the "dead-space" effect [24]; and 2) localized enhancement of the ionization rate. Both reduce the number of possible ionization chains—and, hence, narrow the distribution of the multiplication gain—through spatial localization of the ionization events. Although I²E APDs are reported with $k \sim 0$ at very low gain, this level of performance is not sustained when gain increases beyond $M_{DC} \sim 4$.

Dead space is the physical displacement of an electron or hole inside an electric field. This dead space must pick up sufficient kinetic energy to trigger impact ionization. Secondary electrons and holes that are generated by impact ionization start out with little kinetic energy and must pick up energy from the field in an APD junction before they can impact-ionize and generate progeny carriers. An APD designer can manipulate the dead space inside an APD junction to prevent impact ionization in certain regions and thereby affect the gain statistics. [25],[26],[27],[28] If the

[11] S. Wang, R. Sidhu, X. G. Zheng, X. Li, X. Sun, A. L. Holmes, Jr., and J. C. Campbell, "Low-Noise Avalanche Photodiodes With Graded Impact-Ionization-Engineered Multiplication Region," IEEE Photon. Technol. Lett., vol. 13, pp. 1346–1348, Dec. 2001.

[12] M. M. Hayat, O.-H. Kwon, S. Wang, J. C. Campbell, B. E. A. Saleh, and M. C. Teich, "Boundary Effects on Multiplication Noise in Thin Heterostructure Avalanche Photodiodes: Theory and Experiment," IEEE Trans. Electron. Devices, vol. 49, pp. 2114–2123, Dec. 2002.

[13] S. Wang, J. B. Hurst, F. Ma, R. Sidhu, X. Sun, X. G. Zheng, A. L. Holmes, Jr., A. Huntington, L. A. Coldren, and J. C. Campbell, "Low-Noise Impact-Ionization-Engineered Avalanche Photodiodes Grown on InP Substrates," IEEE Photon. Technol. Lett., vol. 14, pp. 1722–1724, Dec. 2002.

[14] S. Wang, F. Ma, X. Li, R. Sidhu, X. Zheng, X. Sun, A. L. Holmes, Jr., and J. C. Campbell, "Ultra-low noise avalanche photodiodes with a 'centered-well' multiplication region," IEEE J. Quantum Electron., vol. 39, pp. 375–378, Feb. 2003.

[15] O.-H. Kwon, M. M. Hayat, S. Wang, J. C. Campbell, A. Holmes, Jr., Y. Pan, B. E. A. Saleh, and M. C. Teich, "Optimal excess noise reduction in thin heterojunction Al0.6Ga0.4As-GaAs avalanche photodiodes," IEEE J. Quantum Electron., vol. 39, pp. 1287–1296, Oct. 2003.

[16] C. Groves, J. P. R. David, G. J. Rees, and D. S. Ong, "Modeling of avalanche multiplication and noise in heterojunction avalanche photodiodes," J. Appl. Phys., vol. 95, pp. 6245–6251, Jun. 2004.

[17] C. Vèrié, F. Raymond, J. Besson, and T. Nguyen Duy, "Bandgap spin-orbit splitting resonance effects in Hg1-xCdxTe alloys," Journal of Crystal Growth, vol. 59, pp. 342–346, Sep. 1982.

[18] B. Orsal, R. Alabedra, M. Valenza, G. Lecoy, J. Meslage, and C. Y. Boisrobert, "Hg0.4Cd0.6Te 1.55-µm avalanche photodiode noise analysis in the vicinity of resonant impact ionization connected with the spin-orbit split-off band," IEEE Trans. Electron. Devices, vol. ED-35, pp. 101–107, Jan. 1988.

[19] K. A. El-Rub, C. H. Grein, M. E. Flatte, and H. Ehrenreich, "Band structure engineering of superlattice-based short-, mid-, and long-wavelength infrared avalanche photodiodes for improved impact ionization rates," J. Appl. Phys., vol. 92, pp. 3771–3777, Oct. 2002.

[20] F. Ma, X. Li, J. C. Campbell, J. D. Beck, C.-F. Wan, and M. A. Kinch, "Monte Carlo simulations of Hg Cd Te avalanche photodiodes and resonance phenomenon in the multiplication noise," Appl. Phys. Lett., vol. 83, pp. 785–787, Jul. 2003.

[21] M. A. Kinch, J. D. Beck, C.-F. Wan, F. Ma, and J. Campbell, "HgCdTe avalanche photodiodes," J. Electron. Mater., vol. 33, pp. 630–639, Jun. 2004.

[22] A. R. J. Marshall, C. H. Tan, M. J. Steer, and J. P. R. David, "Extremely Low Excess Noise in InAs Electron Avalanche Photodiodes," IEEE Photon. Technol. Lett., vol. 21, pp. 866–868, Jul. 2009.

[23] P. Yuan, S. Wang, X. Sun, X. G. Zheng, A. L. Holmes, Jr., and J. C. Campbell, "Avalanche photodiodes with an impact-ionization-engineered multiplication region," IEEE Photon. Technol. Lett., vol. 12, pp. 1370–1372, Oct. 2000.

[24] B. E. A. Saleh, M. M. Hayat, and M. C. Teich, "Effect of dead space on the excess noise factor and time response of avalanche photodiodes," IEEE Trans. Electron Devices, vol. 37, pp. 1976–1984, Sep. 1990.

[25] P. Yuan et al., "A new look at impact ionization—Part II: Gain and noise in short avalanche photodiodes," IEEE Trans. Electron Devices, vol. 46, pp. 1632–1639, Aug. 1999.

[26] K. F. Li, S. A. Plimmer, J. P. R. David, R. C. Tozer, G. J. Rees, P. N. Robson, C. C. Button, and J. C. Clark, "Low avalanche noise characteristics in thin InP p/sup +/-i-n/sup +/ diodes with electron initiated multiplication," IEEE Photon. Technol. Lett., vol. 11, pp. 364–366, Mar. 1999.

[27] O.-H. Kwon, M. M. Hayat, J.C. Campbell, B. E. A. Saleh, M.C. Teich, "Effect of stochastic dead space on noise in avalanche photodiodes," IEEE Trans. Electron Devices, vol. 51, pp. 693 –700, May 2004.

[28] P. Yuan, H. Chad, K. A. Anselm, C. Lenox, H. Nie, H. L. Holmes, B. G. Streetman, and J. C. Campbell, "Impact ionization characteristics of III-V semiconductors for a wide range of multiplication region thicknesses," IEEE J. Quantum Electron., vol. 36, pp. 198–204, Feb. 2000.

gain distribution of the APD is truncated by use of dead space to eliminate the longer impact-ionization chains, its multiplication noise will be lower. However, absent the longer impact-ionization chains, the mean gain of the APD is also reduced.

A change in semiconductor alloy composition inside the APD junction will result in a change of both the impact-ionization threshold energy and the impact-ionization rate. This makes impact ionization much more likely in some locations and much less likely in others, which narrows the gain distribution. [13],[29] However, like APDs that employ dead-space effects, the spatial localization of impact ionization reduces the number of possible ionization chains and can result in reduced mean avalanche gain.

Increased field strength can produce higher gain from a thin multiplication layer; however, because this approach allows longer ionization chains to fit into the same space, the hole-initiated ionizations create intensified feedback and noise cannot be suppressed. Not only do stronger fields degrade excess noise performance, they also increase dark current leakage by band-to-band and trap-assisted tunneling, which limits the gain over which thin-multiplier designs are effective.

SINGLE-CARRIER-MULTIPLICATION (SCM) APDs

SCM-APD Architecture

The multi-stage single-carrier multiplication (SCM) APD was developed for low-noise, high-gain operation. [30] The SCM APD applies the traditional I^{2}E techniques of dead-space and alloy selection with a tailored electric-field profile to modulate the probability of impact ionization. To achieve high gain and low excess noise simultaneously, SCM APDs are designed using J cascaded asymmetric multiplication regions (Figure 1).

Each heterostructured gain stage is designed for low excess noise at low gains (i.e., $\langle m_j \rangle$ less than 2). By cascading gain stages in the multiplication region, high overall net gain can be achieved while preserving the low excess noise of each gain stage. For example, neglecting any gain resulting from ionization feedback, if a low-noise gain region with

an effective mean gain of $\langle m_j \rangle = 1.7$ is cascaded in a series of five equivalent gain stages, a net gain of $M_{DC} = 14$ is achieved; a seven-stage device achieves a gain of $M_{DC} = 41$; and a 10-stage device reaches a gain of approximately $M_{DC} = 202$.
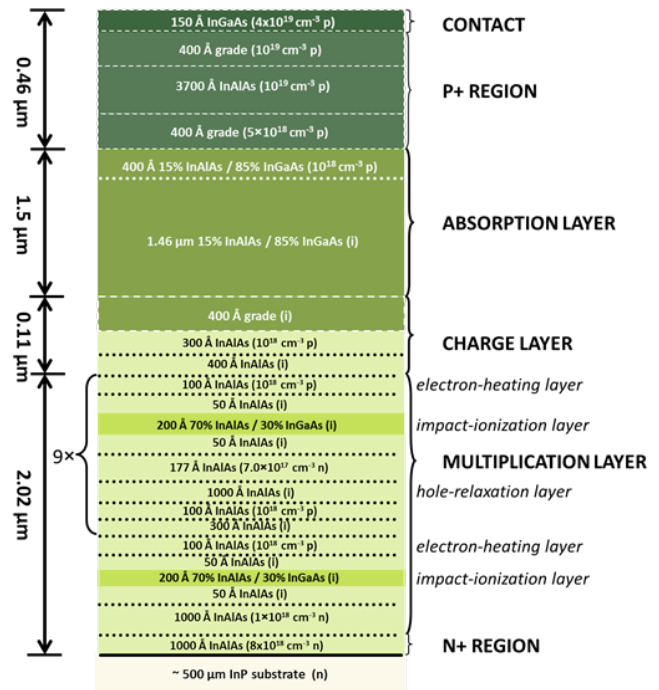

Figure 1: Epitaxial layer structure of an SCM APD with 10 gain stages.

The cascaded multiplier design [31] of the SCM APD is conceptually similar to the "staircase" APD described by Williams, et al., in 1982, [32] but does not rely on band-edge discontinuities at hetero-interfaces to manipulate carrier energy. Instead, doping is used to modulate the electric field inside the multiplying junction, which modulates carrier energy by either accelerating carriers in high-field regions or allowing hot carriers to thermalize in regions of low electric-field strength; alloy composition is varied to pattern the impact-ionization threshold energy. These techniques are applied to reduce the randomness of the multiplication process by suppressing hole-initiated ionizations and enhancing electron-initiated ionizations, while also spatially localizing the latter. Electron-only multiplication eliminates all the impact-ionization chains involving hole avalanche from the universe of possible gain processes, significantly narrowing the gain distribution. Restricting impact ionization

[29] S. Wang, F. Ma, X. Li, R. Sidhu, X. Zheng, X. Sun, A. L. Holmes, Jr., and J. C. Campbell, "Ultra-low noise avalanche photodiodes with a centered-well multiplication region," IEEE. J. Quantum Electron., vol. 39, pp. 375–378, Feb. 2003.

[30] G. M. Williams, D. A Ramirez, M. M. Hayat, and A.S. Huntington, Time resolved gain and excess noise properties of InGaAs/InAlAs avalanche photodiodes with cascaded discrete gain layer multiplication regions," J Appl Phys, vol. 113, p. 093705, Mar. 2013.

[31] A. Huntington, United States Patent 7,432,537, 2008.

[32] G. F. Williams, F. Capasso, and W. T. Tsang, "The graded bandgap multilayer avalanche photodiode: A new low-noise detector," IEEE Electron Device Lett., vol. EDL-3, pp. 71–73, Mar. 1982.

to small regions of the junction likewise eliminates certain gain processes that would otherwise contribute to gain variability. Thus, the cascaded multiplier design suppresses excess multiplication noise by physically eliminating many of the gain processes that contribute to gain variability.

Within each gain stage, the asymmetric electric-field profile is responsible for suppressing hole-initiated impact ionization. Carriers impact-ionize most readily in the AlGaInAs layer, which combines a lower impact-ionization threshold with the highest electric-field strength. However, the impact-ionization layer is sized to be approximately the size of the carrier dead space, meaning that carriers that are cold when injected into that layer are unlikely to pick up sufficient energy to ionize before they exit the layer. The electric-field profile is patterned so that electrons are preheated prior to injection into the impact-ionization layer, whereas holes are injected cold.

This structure would not achieve noise suppression if the holes were to pick up kinetic energy in one gain stage and enter into an adjacent stage with sufficient energy to impact-ionize. Therefore, the gain stages are separated by low-field carrier relaxation regions in which both electrons and holes lose their accumulated kinetic energy through random phonon scattering. In this way, the holes generated in later gain stages drift back through the earlier gain stages, to the anode, without impact ionizing.

SCM-APD Device Simulation

Monte Carlo Models of SCM APDs

To develop the multi-stage APD design and to aid in the design of the SCM APD, a quasi-empirical Monte Carlo simulator of impact ionization in arbitrary junction designs was written. The Monte Carlo simulator treats material-dependent and field-dependent variation in ionization threshold energy and ionization rates, and tracks carrier energy effects such as dead space and relaxation. It is quasi-empirical in the sense that it does not directly calculate scattering rates; rather, it relies on simple field-dependent exponential models of the impact-ionization rate of active carriers, impact-ionization threshold energies, and estimates of carrier mean free path published by others. A recursive algorithm is used to simulate ionization chains.

The spatial occurrence and number of hole-initiated and electron-initiated impact-ionization events from a 100-trial subset of a 20,000-trial simulation of a 10-stage SCM APD operating at an average gain of M_{DC} = 599 are plotted in Figure 2.
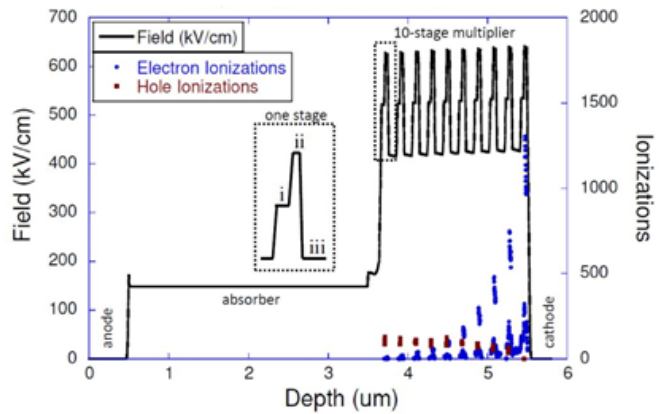

Figure 2: Spatial distribution of electron- and hole-initiated impact ionization (points) plotted against the electric-field profile for a 100-trial sample of a 20,000-trial Monte Carlo simulation of a 10-stage SCM APD operating at a mean gain of M_{DC}= 599. An excess noise of $F(M_{DC})$ = 6.47 was simulated.

It should be remarked that the electric-field profile found by the band-edge simulator is based on an idealization of the dopant distribution in which doping concentration is uniform and doping is confined to the epitaxial layers into which the dopant species were introduced during growth.

In Figure 2, electrons drift from left to right, from anode to cathode, and holes drift from right to left; photocarrier pairs are initially generated in the InGaAs absorber of the APD such that only photoelectrons are injected into the multiplier. As shown in the inset in Figure 2, the purpose of the first layer of one of the repeating asymmetric gain stages (labeled "i") is to preheat electrons prior to injection into the impact-ionization layer (labeled "ii"), while keeping the electric field low enough that holes exiting the impact-ionization layer are unlikely to ionize. The impact-ionization layer (labeled "ii") is characterized by both a higher field and a semiconductor material ($Al_{0.335}Ga_{0.140}In_{0.525}As$) with a smaller bandgap (1.20 eV versus 1.46 eV) than the surrounding $In_{0.521}Al_{0.479}As$. The combination of a strong electric field and a lower impact-ionization threshold energy in layer (ii) promotes impact-ionization by hot electrons injected from layer (i), but the layer is designed to be too thin for the cold holes injected from the energy relaxation layer (labeled "iii") to pick up sufficient energy to ionize. Finally, layer (iii), is characterized by an electric field sufficiently low that individual hole carriers spend very little time with kinetic energy in excess of the ionization threshold; this suppresses the probability of hole ionization, so that low-noise avalanche multiplication is achieved. [30]

Carriers traveling at the saturation drift velocity are expected to have mean kinetic energy on the order of the optical phonon energy of 30 – 40 meV, whereas the impact-ionization threshold energy is approximately 1 eV in InGaAs or 2 eV in InAlAs. Within region (iii), the impact-ionization rate is negligible because the mean free path between phonon

collisions is short compared to the displacement in the field required to accumulate the impact-ionization threshold energy, such that individual carriers spend very little time with kinetic energy in excess of the ionization threshold. In contrast, at the electric-field strength characteristic of the impact-ionization layer, carriers have a reasonable probability of accumulating the threshold energy so that they ionize before losing energy through scattering. Thus, the function of region (iii) is to reset the dead space of active carriers exiting impact-ionization layers while minimizing the likelihood that those active carriers will impact-ionize before scattering; this helps localize the avalanche to the impact-ionization layers and prevents injection of active holes into impact-ionization layers.

For the specific simulation of the 10-stage SCM APD biased for M_{DC} = 599 presented in Figure 2, the Monte Carlo model predicts an excess noise factor of F = 6.47, which, using Equation 9 is equivalent to a bulk multiplier with an effective ratio of hole-to-electron ionization rates of k ~ 0.007. Good agreement between modeled and measured results has been obtained over a number of different designs, gain stages, and operating biases. However, the limitations of implementation and approximation should be recognized. The device structure analyzed by the Monte Carlo model is an idealization of what can be grown epitaxially. The use of a hard dead space, a fixed energy relaxation length, and impact-ionization rates for active carriers that are independent of carrier energy are all simplifying assumptions. As such, the Monte Carlo model was useful for designing the SCM APD and interpreting measurements on SCM APDs, although it uses empirical parameters to obtain accurate results, so it ought not be regarded to be as quantitatively predictive as a full-band Monte Carlo model.

Dead-Space Multiplication Theory (DSMT) Numeric Models of SCM APDs

To validate the Monte Carlo model used in this work, University of New Mexico (UNM) researchers used the same impact-ionization threshold energies and field-dependent rate models to perform numeric simulations. The purpose of the UNM calculations was to use a separate methodology to analyze the SCM-APD design. The parameters used by both models to calculate the field-dependent impact-ionization rates for active carriers (i.e., those with kinetic energy in excess of the impact-ionization threshold), are summarized in Table 1, taken from Saleh, et al., [33],[34] and Pearsall. [35]

Table 1: Material Parameters to Calculate Impact-Ionization Rates; $\alpha, \beta = A \exp[-(B/E_{field})^m]$

Material	A (cm^{-1})	B (V/cm)	m	Carrier
InGaAs	1.8×10^7	1.95×10^6	1	Electrons
	2.56×10^7	2.2×10^6	1	Holes
InAlAs	4.17×10^6	2.09×10^6	1.2	Electrons
	2.65×10^6	2.79×10^6	1.07	Holes

The prefactors, A, for InGaAs were reduced by a factor of 2.85 from those published by Pearsall to fit the Monte Carlo model calculation of excess noise factor to the measurements for the I2E structure reported by Wang, et al. [13] This method was chosen due to a lack (as of the time of publication) of published impact-ionization rate models for the quaternary alloy $Al_{0.335}Ga_{0.140}In_{0.525}As$ used in the SCM-APD multiplier; however, excess noise data, published by Wang, et al., are available for an I2E APD that uses the same alloy composition. The quaternary alloy is implemented as a blend of the lattice-matched ternary alloys $In_{0.52}Al_{0.48}As$ and $In_{0.53}Ga_{0.47}As$, so ionization coefficients for the quaternary AlGaInAs alloy were estimated as the appropriate linear combination of the ionization coefficients for the lattice-matched ternary alloys. The 2.85× reduction of the prefactors is within the range of ambiguity for $In_{0.53}Ga_{0.47}As$ found by Osaka, et al., [36] who remark that Pearsall's rate coefficients for InGaAs are approximately one order of magnitude larger than those they measured.

The threshold energies used to calculate the dead space, also taken from Saleh, et al., are shown in Table 2.

Table 2: Threshold Energies Used to Calculate the Dead-Space Profile

Material	Threshold Energy (eV)	Carrier
InGaAs	1.20	Electrons
	1.00	Holes
InAlAs	2.15	Electrons
	2.30	Holes

[33] M. A. Saleh, M. M. Hayat, O.-H. Kwon, A. L. Holmes, Jr., J. C. Campbell, B. E. A. Saleh and M. C. Teich, " Breakdown voltage in thin III–V avalanche photodiodes," Applied Physics Letters, vol. 79, pp. 4037–4039, Dec. 2001.

[34] M. A. Saleh, M. M. Hayat, B. E. A. Saleh, and M. C. Teich, "Dead-space-based theory correctly predicts excess noise factor for thin GaAs and AlGaAs avalanche photodiodes," IEEE Trans. Electron Devices, vol. 47, p. 625, Mar. 2000.

[35] T. P. Pearsall, "Impact ionization rates for electrons and holes in Ga0.47In0.53As," Applied Physics Letters, vol. 36, pp. 218–220, Feb. 1980.

[36] F. Osaka, T. Mikawa, and T. Kaneda, "Impact ionization coefficients of electrons and holes in (100)-oriented Ga1-xInxAsyP1-y," IEEE Journal of Quantum Electronics, vol. QE-21, pp. 1326–1338, Sep. 1985.

To accommodate for carrier relaxation due to phonon scattering, the nonlocalized ionization coefficients have been modified in this paper into new types of ionization coefficients, which are referred to here as the "scattering-aware" ionization coefficients, which were integrated into a recursive dead-space multiplication theory (DSMT) impact-ionization model [12],[37] to capture carrier "reset" effects. Once these scattering-aware ionization coefficients are calculated, they are substituted for the nonlocalized ionization coefficients in the expression for the probability density function of the distance to the first ionization.

Notion of Scattering-Aware Ionization Coefficients

The model for the probability density function of the distance to the first impact ionization has been modified to incorporate a relaxation mechanism for suppressing the impact ionizations triggered by one species of carrier, such as through phonon scattering. Specifically, it is assumed that a carrier loses its energy and ceases to be able to impact-ionize if it travels a certain nominal distance during which the electric field is below a certain threshold (30 nm below 103 V/cm in these studies). [38] More precisely, it is assumed that the energy accumulated by a carrier is reset to zero once the carrier travels the nominal distance under a field that falls below a certain threshold.

The scattering-aware ionization coefficient for holes and electrons, $\bar{\alpha}(y \mid x)$ and $\bar{\beta}(y \mid x)$, respectively, are defined as follows: $\bar{\alpha}(y \mid x)$ is the ionization coefficient at y for an electron that has zero energy at location x, where $x < y$; and $\bar{\beta}(y \mid x)$ is the ionization coefficient at y for a hole that has zero energy at location x, with $x > y$. Note that, unlike the nonlocalized ionization coefficients, these coefficients are dependent on the entire field profile from x to y, not just the field at y.

The scattering-aware ionization coefficients are calculated as follows: Let $d_e(x)$ and $d_h(x)$ denote the dead space that an electron and hole, respectively, created at location x in the multiplication region must travel before it can accumulate enough energy to reach the ionization threshold of the material. For an electron starting at location x with zero energy reserve, $\bar{\alpha}(y \mid x) = 0$ if $y < x + d_e(x)$. However, if $y \geq x + d_e(x)$, then the last point, s, is found; this is the point at which the energy of the electron was reset to zero. Then, it is checked whether the electron has travelled the dead space $d_e(s)$ beyond the point s. If indeed it has travelled

$d_e(s)$ beyond s, then $\bar{\alpha}(y \mid x) = \alpha(y)$, where $\alpha(y)$ is the usual nonlocalized ionization coefficient (also termed enabled ionization coefficients in the work of McIntyre [2]). On the other hand, if the electron has not travelled distance $d_e(s)$ beyond s, then $\bar{\alpha}(y \mid x) = 0$. The scattering-aware ionization coefficient for the holes is calculated similarly. Once the scattering-aware ionization coefficients are calculated, they are substituted for the nonlocalized ionization coefficients in the expression for the probability density function of the distance to the first ionization using the shifted, exponential probability density function used by the DSMT. [1] The scattering-aware probability density function for $y \geq x$ is given by:

Equation 5:

$$
h_e(y \mid x) = \begin{cases} \bar{\alpha}(y \mid x) \exp\left(- \int_{x+d_e(x)}^{y} \bar{\alpha}(z \mid x) \, dz \right), & w \geq y \geq x + d_e(x) \\ 0, & 0 < y < x + d_e(x) \end{cases} ;
$$

and the scattering-aware probability density function for $y \leq x$ is given by:

Equation 6:

$$
h_h(y \mid x) = \begin{cases} \bar{\beta}(y \mid x) \exp\left(- \int_{y}^{x-d_h(x)} \beta(z \mid x) \, dz \right), & 0 < y < x - d_h(x) \\ 0, & x \geq y > x - d_h(x) \end{cases} .
$$

Note that the scattering-aware ionization coefficients capture scattering in a more-detailed manner than either the "bulk" (localized) or the enabled and history-dependent ionization coefficients. This is because the scattering-aware coefficients track the history of the electric field experienced by a carrier as it is transported. For example, although the nonlocalized ionization coefficient obtained when the DSMT model is fit to the experimental F vs. M_{DC} data [39] is able to capture scattering effects statistically, the scattering-aware coefficients have an added feature that enables an active reset of the energy of the carriers as they are transported. This method is more suitable for layered multiplication regions where the locations of high and low scattering are controlled in space via changes in the electric field.

[37] M. M. Hayat, B. E. A. Saleh, and M. C. Teich, "Effect of dead space on gain and noise of double-carrier-multiplication avalanche photodiodes," IEEE Trans. Electron Devices, vol. 39, pp. 546–552, Mar. 1992.

[38] J. P. R. David, J. Allma, A. R. Adams, J. S. Roberts, R. Grey, G. J. Rees, and P. N. Robson, "Avalanche breakdown in AlxGa1-xAs alloys and Al0.3Ga0.7As/GaAs multilayers," Applied Physics Letters, vol. 66, pp. 2876–2878, May 1995.

[39] M. A. Saleh, M. M. Hayat, B. E. A. Saleh, and M. C. Teich, "Dead-space-based theory correctly predicts excess noise factor for thin GaAs and AlGaAs avalanche photodiodes," IEEE Trans. Electron Devices, vol. 47, pp. 625–633, Mar. 2000.

Scattering-Aware DSMT Applied to SCM-APD Design

The nonlocalized and scattering-aware ionization coefficients for electrons, α, and holes, β, across the structure are shown in Figure 3, for cases where phonon scattering is either neglected (dashed lines) or considered (solid lines).

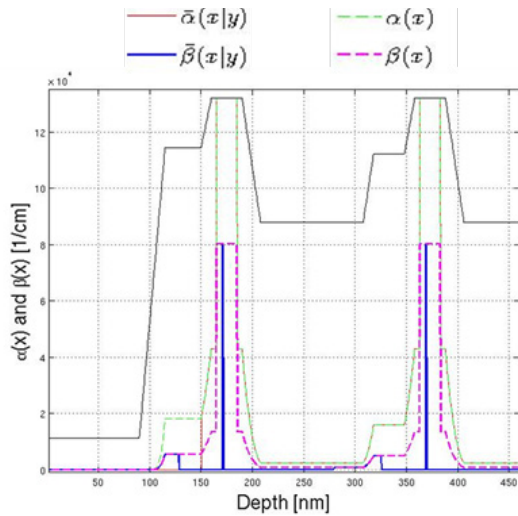Figure 3: The impact-ionization coefficients for electrons, α, and holes, β, are shown across the structure for cases where phonon scattering is considered (solid curves) or neglected (dashed curves). The bias conditions are for $M_{DC} = 937$. The plot is a zoomed view of the impact ionization in two stages.

The inclusion of phonon scattering in the numerical models results in a tighter spatial distribution of electron ionization events in each gain stage and simultaneously reduces the occurrence of hole ionization events throughout the structure. When the phonon scattering in the energy relaxation region (Figure 2, inset "iii") is considered, the numeric models show that electrons ionize almost immediately upon entering the high electric-field region of the impact-ionization layer (Figure 2, inset "ii"), but have a low probability of ionizing elsewhere in the gain stage. When phonon scattering is considered, the hole ionization rate is negligible throughout the entire gain stage. The scattering-aware ionization rates more closely resemble the Monte Carlo plots of Figure 2, whereas the models that do not include phonon scattering have ionization rates of larger magnitude and wider spatial extent for both holes and electrons.

The dead-space profile calculated for electrons and holes, taking into account phonon scattering effects over a few periods of a 10-stage SCM-APD multiplier, is shown in Figure 4. The excess noise vs. gain characteristics predicted by the DSMT for a 10-gain-stage SCM APD are shown in Figure 5.
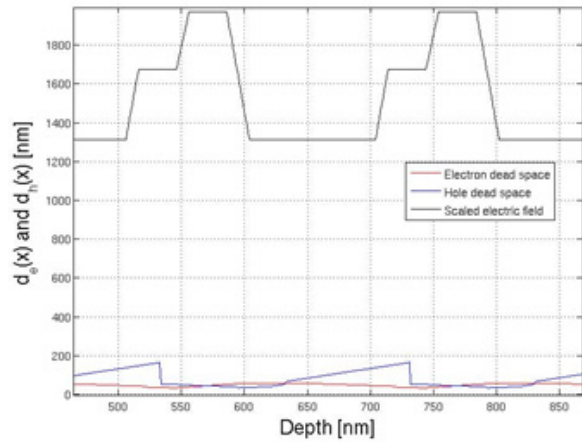

Figure 4: Dead-space profile of electrons and holes in a two-gain-stage region of the SCM-APD multiplication region. A plot of the electric field (arbitrary units) is shown for reference.
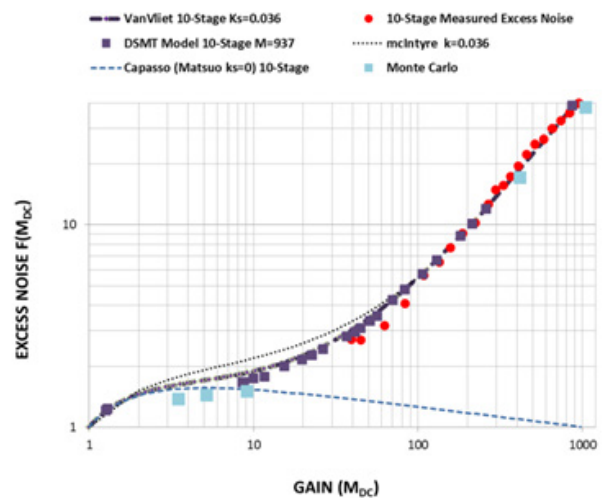

Figure 5: Plots of excess noise predicted by the DSMT numeric model for a 10-stage SCM APD operated at a bias of $M_{DC} = 937$ and the Monte Carlo-modeled results ($M_{DC} = 1200$) compared to measured excess noise data for a 10-stage SCM APD ($M_{DC} = 1200$). Also plotted are the McIntyre model (Equation 4, for $k = 0.36$), the Van Vliet model (Equation 9, for $k_s = 0.036$) for a two-carrier ionization 10-stage SCM APD, and the Capasso model (Equation 8) for an ideal 10-stage device.

The DSMT and Monte Carlo models of Figure 5 predict similar performance and are in good agreement with the empirically measured results. Also plotted in Figure 5 are the analytical McIntyre-modeled excess noise values from Equation 4, $k = 0.036$. It is to be expected, at most biases, that the empirical and numerically modeled results do not match Equation 4 as the SCM-APD design differs from that of a bulk, dead-space-free APD assumed by McIntyre. [2] The data converge with the McIntyre formula only at DC gain levels exceeding approximately 125.

Analytical Discrete Low-Gain Multi-Layer APD Models

For an ideal SCM-APD device without hole feedback, $F(M_{DC})$ can be expressed in terms of the electron count mean and variance that result from a single primary relation event, and the excess noise factor is only due to those carriers that cannot ionize, δ, where $\delta = 1 - P_e$, where P_e is the probability that the electron ionizes in each gain stage. In this specialized case, the gain is:

Equation 7:

$$M_{DC} = (2 - \delta)^J,$$

where J is the number of gain stages. The excess noise factor after Capasso[40] is:

Equation 8:

$$F(J, \delta) = 1 + \frac{\delta[1 - (2-\delta)^{-J}]}{(2-\delta)}.$$

Note that in Equation 8, $F(J,\delta)$ is < 2 for any J. When $P = 1$, in the absence of carrier fluctuations, $var\,(J,\delta) = \delta(1 - \delta) = 0$ and $F = 1.0$. This cannot be achieved in a conventional APD at high gain even if one of the ionization coefficients is zero. However, these conditions may apply to the SCM APD at low biases, assuming there is no significant hole ionization feedback.

Assuming two-carrier ionization multiplication processes, in a low-gain limit, the discrete nature of the ionization process for both carriers must be considered. The analyses of Van Vliet[41] and Lukaszek[42] show that this leads to a reduced excess noise factor compared to McIntyre predictions, for sufficiently low gains. When both hole- and electron-ionization are included in a multi-stage discretized APD, the excess noise can be approximated as[41],[43]:

Equation 9:

$$F(J, \delta) = 1 + \frac{(1 - \frac{1}{\langle M_{DC}\rangle})(1 - k_s)}{2 + P(1 - k_s)} \times$$
$$\left[-P + 2\frac{(1-k_sP^2)}{(1+k_sP)}\left(\langle M_{DC}\rangle k_s \frac{(1+P)}{(1-k_s)} + \frac{1}{1+P}\right)\right],$$

where $k_s = Q/P$ is the ratio of the hole-ionization probability per gain stage Q, to the electron-ionization probability per gain stage P, and the mean output gain, $\langle M_{DC}\rangle$, is calculated by:

Equation 10:

$$M_{DC}(J) = \frac{(1+P)^J(1-k_s)}{(1+k_sP)^{J+1} - k_s(1+P)^{J+1}}.$$

The Van Vliet model (Equation 9, $k_s = 0.036$) is plotted in Figure 5 as a function of gain calculated by Equation 10 ($k_s = 0.036$) over all possible values of P. The analytical models show good agreement with the Monte Carlo and DSMT simulations over most bias conditions, and approximate the McIntyre models only at higher biases (i.e., $M_{DC} > 125$).

The agreement between Equation 9 and the numeric DSMT simulations is not surprising, as it has been shown previously that an SCM APD with dead space can be approximated by a superlattice (ideal, discrete multilayer) APD for which the separation between the layers is the dead space, and the ionization probability per layer is obtained by matching the gains of the two devices.[44] However, unlike the analytical excess noise models of Equation 4 and and Equation 9, the DSMT does not involve any fitting parameters (i.e., k and k_s) to the data; it only uses universal parameters for the nonlocalized ionization coefficients, ionization threshold energies of materials, and simple phonon-scattering rules.

[40] F. Capasso, W. T. Tsang, and G. F. Williams, "Staircase solid-state photomultipliers and avalanche photodiodes with enhanced ionization rates ratio," IEEE. Trans. Electron. Devices, vol. ED-30, pp. 381–390, Apr. 1983.

[41] K. M. van Vliet, A. Friedmann, and L. M. Rucker, "Theory of carrier multiplication and noise in avalanche devices—Part II: Two-carrier processes," IEEE Trans. Electron Devices, vol. ED-26, pp. 752–764, May 1979.

[42] W. A. Lukaszek, A. van der Ziel, and E. R. Chenette, "Investigation of the transition from tunneling to impact ionization multiplication in silicon p-n junctions," Solid-State Electronics, vol. 19, p. 57, Jan. 1976.

[43] M. C. Teich, K. Matsuo, and B.E.A. Saleh, "Excess noise factors for conventional and superlattice avalanche photodiodes and photomultiplier tubes," IEEE Journal of Quantum Electronics, vol. 22, pp. 1184–1193, Aug. 1986.

[44] B. E. A. Saleh, M. M. Hayat, and M. C. Teich, "Effect of dead space on the excess noise factor and time response of avalanche photodiodes," IEEE Trans. Electron Devices, vol. 37, pp. 1976–1984, Sep. 1990.

SCM-APD DEVICE DESIGN AND FABRICATION

SCM-APD Epitaxial Growth

SCM APDs with the multiplier design presented in Figure 1 were grown by molecular beam epitaxy (MBE) on 2-inch N-type (100)-oriented InP substrates. Three-, 5-, 6-, 7- and 10-stage SCM APDs were grown with $Al_{0.07}Ga_{0.40}In_{0.53}As$ absorbers; and 7-stage SCM APDs were grown with $In_{0.53}Ga_{0.47}As$ absorbers.

Physical implementation of this design requires that the P- and N-type doping within each multiplying stage balance nearly quantitatively. A net excess of space charge in the multiplier effectively adds to or subtracts from the doping of the charge or "field control" layer. This changes the "punch-through" voltage of the APD, which is the bias at which the growing depletion region penetrates the charge layer interposed between the multiplication layer and the narrow-gap absorber to which photocarrier generation is confined. Early punch through occurs with tunnel leakage in the absorber, and late punch through results in breakdown without photosensitivity.

Dopant cell flux, growth temperature, and growth rate tend to be very consistent for adjacent epitaxial layers in a single MBE growth run, so doping errors during SCM-APD multiplier growth are systematic rather than random. The doping precision required to balance SCM-APD multipliers cannot always be achieved by routine methods, so a series of SCM-APD wafers are normally grown in which the thickness of the N-type layer is incrementally varied relative to a constant P-type layer specification. This method, aided by the systematic nature of the doping mismatch, generally achieves good results.

Device Fabrication

Back-illuminated photodiodes of varying diameter were etched in MBE-grown epitaxial material. Anode pixel contacts on top of the diode mesas and annular cathode contacts at the base of the mesas were patterned. A cleanup etch was then performed to remove surface material contaminated by the contact metallization. Next, a rapid thermal anneal was performed. The mesa sidewalls were then encapsulated with a polymer. Polishing was then performed. Last, a two-layer broadband anti-reflection coating was applied to the backside of the InP substrates.

EXPERIMENTAL RESULTS

Test Procedures

Gain curves were generated from the current-voltage (I-V) characteristics of the APDs. Initial I-V screening was performed by needle-probe of the on-wafer APDs; later, individual packaged parts were fixtured and tested. In either case, a semiconductor parameter analyzer was used to sweep applied reverse bias and read the current. Stable, switchable illumination was projected onto the detector under test (DUT) by either a light-emitting diode (for on-wafer testing) or a stabilized fiber-coupled 1064 nm diode laser (for testing of packaged components). Room-temperature on-wafer testing was performed in a dark box housing a probe station. The packaged parts were tested inside a vacuum cryochamber.

Following burn-in under bias, during which the I-V characteristics of the APD stabilized, light and dark I-V and capacitance-voltage (CV) curves were measured at 300 K. The dark current was measured directly, and the avalanche gain of the photocurrent was calculated using:

Equation 11:

$$M(V) = \frac{I_{light}(V) - I_{dark}(V)}{I_{light}(V_{M=1}) - I_{dark}(V_{M=1})}.$$

In Equation 11, $V_{M=1}$ is the unity-gain reference point. Correct identification of $V_{M=1}$ is critical to the scaling of both gain and excess noise data because it is important to measure photocurrent and noise power levels relative to their unity gain values.

In InGaAs APDs, the depleted volume from which the multiplying junction collects primary carriers initially grows with reverse bias. Maximum collection of primary photocarriers normally occurs just after punch through . The unity-gain condition is normally identifiable as a plateau in the photocurrent immediately after punch through, where collection of primary photocarriers is at a maximum, and before the impact-ionization process has turned on in the multiplier. However, if a narrow-gap cap layer is used to promote an ohmic contact, then a second source of photocarriers may be present in a top-illuminated structure. Photocarrier collection will continue to grow slightly as the depletion layer expands into the absorber, overlapping with the diffusion tail of photogenerated carriers from the cap. This can lead to a small, double plateau in the measured photocurrent, and incorrect scaling of gain and noise data if $V_{M=1}$ is chosen before the second plateau. In other cases, the multiplier of an APD will already be operating above unity gain by the time maximum photocarrier collection is achieved. In this case, the unity-gain reference photocurrent cannot be measured directly, and the scaling of gain and noise measurements will be less accurate. In such cases, measurement of spectral responsivity can help estimate the gain at punch through based on the quantum efficiency expected of the absorber design.

Room-temperature excess noise measurements were performed on ceramic submount-packaged APDs fixtured inside a dark box. Bias was applied to the contacts of the sub-mounted APDs using a semiconductor parameter analyzer and a microwave probe (50 Ω). In the excess noise test, a bias-T coupled the DC component of the diode current to the SPA and sent the AC component to a low-noise amplifier. The amplifier fed either a spectrum analyzer or a noise figure meter. In this way, both the average DC gain (M_{DC}, calculated from the DC component of the photocurrent) and the noise power spectral intensity at a given frequency (S_P, calculated from the AC component) were read simultaneously. A spectrum analyzer was used to select a handful of low environmental noise frequencies within the 30 to 100 MHz band, and a noise figure meter was used to make calibrated noise power measurements.

Noise power measurements were taken both in dark and illuminated conditions. The fiber-delivered optical signals under-filled the active area of the SCM APD and the optical power level was monitored, via a fiber splitter, using a calibrated InGaAs reference photodiode and associated optical power meter.

A light level was selected that generated photocurrent approximately 10 times the level of the dark current. This isolated the noise power of the photocurrent from the noise power of the dark current and thereby allowed the noise power of the dark current to be subtracted. To ensure that the optical source dominated the noise performance, noise statistics were calculated at unity gain and every other bias used for testing, using a series of optical power levels. Calibrated responsivity measurements were also taken during testing to confirm the signal gain and to detect any nonlinear saturation effects.

The noise figure meter outputs the noise power spectral intensity measurements (S_P in W/Hz). To convert these measurements to noise current spectral intensity (S_I in A^2/Hz), the impedance of the test circuit must be found. To obtain the most direct measurement of the relevant impedance, DUT impedance in isolation was not measured. Rather, the noise measurement at unity gain was used for this normalization because this measurement includes effects from the mounting of the detector, its interaction with the preamplifier and noise figure meter, and anything specific to the frequency band used for the noise power measurement. The normalization was accomplished using Schottky's theorem, $S_I = 2qI$ (A^2/Hz), and direct measurement of the DC photocurrent, I:

Equation 12:

$$R = S_P / S_I = S_P / (2qI).$$

Between 20 and 30 independent measurements of the light and dark noise power at unity gain were used to find R. Subsequently, noise current spectral intensity was measured at a variety of different values of M_{DC}, using 10 independent measurements of light and dark noise power for each gain point. Finally, the excess noise factor was calculated using the noise current spectral intensity theorem for avalanche multiplication, using:

Equation 13:

$$S_I = 2\ q\ I\ M^2 F(M_{DC}).$$

This methodology was selected to enable accurate measurement of the impedance of the test circuit under the same conditions as the noise measurements, so that the generated excess noise curve would be normalized for $F(M_{DC}) = 1$ at $M_{DC} = 1$ and the data would satisfy Schottky's theorem.

However, experimental variation is always associated with the noise power measurement, so this measurement of the test circuit impedance is not absolutely accurate. Accordingly, some scatter in the $F(M_{DC})$ data is generally found at higher gain. This is an experimental limitation that was minimized by averaging a large number of noise measurements and selecting relatively "quiet" RF frequency bands in which to make the measurements; however, this scatter cannot be eliminated entirely.

Calibration of the excess noise measurements is sensitive to identification of the point in the APD I-V characteristic where full collection of primary photocarriers is reached and the gain at that point. When full collection of primary photocarriers occurs at a reverse bias for which $M_{DC} > 1$, Equation 11 is no longer valid, and using Equation 12 to estimate R requires a value to be assumed for the APD excess noise factor at the reference gain. These requirements are problematic because R scales all of the noise power measurements that are subsequently used to measure the excess noise at higher gain. Because of the forms of Equation 4 and Equation 9, the excess noise factors at low gain are not especially sensitive to the value of k that is assumed. For instance, for $k = 0.3$ (bulk InAlAs) at $M_{DC} = 1.5$, $F = 1.38$; whereas, for $k = 0.02$ (a good silicon APD) at $M_{DC} = 1.5$, $F = 1.34$. Thus, as a practical matter, the test-system impedance-calibration problems introduced by punch through above unity gain are manageable if the gain at punch through is sufficiently low.

Potential errors were minimized by using the C-V measurements to confirm punch through. The unity gain responsivity values were also compared to SCM APDs with the same absorption layer composition and thickness, albeit

with a different number of gain stages, and device quantum efficiencies were verified to be within the range of previously manufactured APDs with similar absorption layers (i.e., 70% to 90%, depending on composition and wavelength).

To achieve good signal-to-noise performance and to avoid saturation effects, gain measurements were taken at a number of light levels. The relative gain and excess noise at each bias were verified by fitting gain-normalized optical power spectral density curves to the unity gain measurement (i.e., shot-noise limited), which confirmed the consistency of the gain measurements. Gain was further confirmed by gain-normalized plots of the trap-assisted-tunneling dominated dark current to the activation energy of the traps.

The I-V curves for the various multigain-stage devices are shown in Figure 6. The onset of punch through in the 5-stage device is quite evident and, using the responsivity measurements of the 5-stage AlGaInAs absorption layer device at unity gain, the gain of the 10-stage device—where the onset of punch through occurs after unity gain—can be determined more accurately.

Punch-through of the 7-stage InGaAs absorption layer APD is also evident and was further calibrated by comparing the unity gain responsivity (see Figure 7) to the comparable-thickness InGaAs absorption layers of conventional APDs (i.e., those with separate absorption, charge, and multiplication layers) fabricated using the same process.
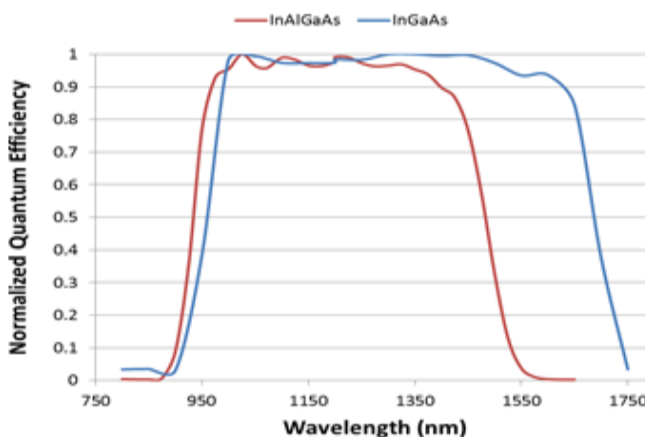

Figure 7: Normalized quantum efficiency (QE) measurements for the InGaAs (5-stage and 7-stage) and InAlGaAs (10-stage) SCM APDs.

MEASURED SCM-APD NOISE PERFORMANCE

In all, several hundred devices were tested, and excess noise measurements were performed on approximately 30 SCM APDs selected from different wafers manufactured on several lots. The devices were tested over the 77 K to 295 K temperature range.

The 295 K excess noise measurements for the 5-stage, 7-stage, and 10-stage SCM APDs are shown as a function of mean gain in Figure 8, wherein the low-gain excess noise measurements are plotted on a linear scale, and the excess noise measurements over the full gain range of the SCM APDs are plotted on a log-log scale. Also plotted in Figure 8 are: the numerically modeled data for a 10-stage SCM APD with an $M_{DC} = 937$ bias; McIntyre-modeled data (i.e., Equation 4, for $k = 0$, 0.2, and 0.36); Van Vliet-modeled data for an SCM APD (i.e., Equation 9, for $k_s = 0.036$), and Capasso-modeled data for ideal (no ionization feedback) 5-, 7-, and 10-stage SCM APDs (i.e., Equation 8).

Figure 6: Measured I-V and gain curves for 5-, 7-, and 10-stage SCM-APD devices, taken at 300 K: The light levels are chosen so that the noise is dominated by the statistics of the photocurrent but does not saturate the detector at the highest gain bias settings. For the 10-stage device, four different light levels were used so that good signal-to-noise performance was achieved in the measurements. Only the lowest light level that did not saturate the detector over the full range of biases is shown. Notably, the 10-stage device did not exhibit breakdown behavior.
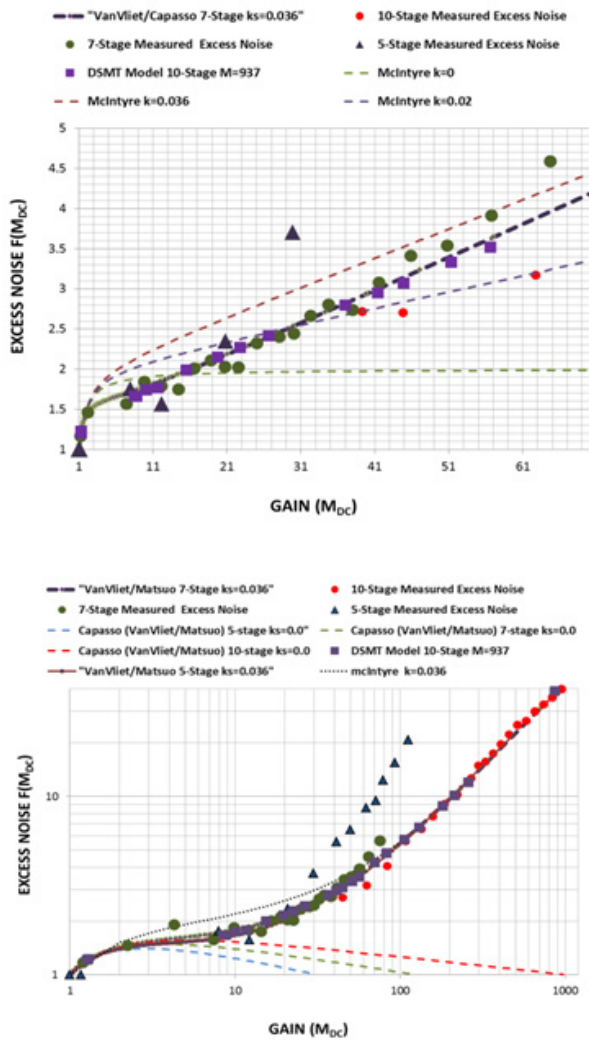
Figure 8: Plots of excess noise measurements for the 5-, 7-, and 10-stage SCM APDs plotted on a linear scale for gains below 70 (top) and on a log-log scale for the entire gain range (bottom). Also plotted is the performance predicted by: DSMT numerically modeled data (10-stage SCM APD with M_{DC} = 937); Van Vliet-modeled data (i.e., Equation 9) for a 7-stage device with k_s = 0.036; and McIntyre-modeled data (i.e., Equation 4, for k = 0, 0.2, and 0.036). In the bottom plot, the measured data are shown with the Capasso model (i.e., Equation 8) for an ideal 5-, 7-, and 10-stage SCM APD, the Van Vliet model (i.e., Equation 9, for k_s = 0.036), and the McIntyre model (i.e., Equation 4, for k = 0.036).

DISCUSSION OF RESULTS

In Figure 5, it was shown that the measured 10-stage SCM-APD excess noise data match the predictions of DSMT numeric models, Monte Carlo models, and analytical discrete multilayer APD models (i.e., Equation 9). The measured excess noise curves shown in Figure 8 further display the design principles employed in the SCM-APD design.

Gain and Excess Noise Performance

The excess noise data of Figure 8 include the performance of 5-stage, 7-stage, and 10-stage devices and provide further insight into the noise properties and bias-dependent (i.e., electric-field dependent) carrier dynamics of SCM APDs. Five noise domains are evident in the excess noise data.

Single-Carrier-Dominated Multiplication

At the lowest biases, a majority of the gain results from the current induced in the circuits by the initial photoelectron and the ionizing electron progeny as they traverse the gain stages during the photoelectron transit of the multiplication region. Assuming minimal hole ionization feedback, the excess noise in this region can be characterized by the Capasso model in Equation 8. This region is best represented by the 7-stage SCM-APD data in Figure 8. The measured data appear to depart from Equation 8 at approximately M_{DC} = 5. Using Equation 7, this would suggest P = 0.25. At higher biases, from the fit of Equation 9, where k_s = 0.036, the probability of hole ionization can be estimated to be approximately Q = 0.009. The largest number of electron-hole pairs are created at the last gain stage. Given that there are $(J - 1)$ gain stages where the holes can potentially ionize during the drift toward the P+ contact, there is an insufficient probability of feedback to sustain further avalanche at this stage. Thus, it can be assumed that the majority of the gain occurs during the initial transit time of the photoelectron.

Discrete Multiplication with Low Gain Per Stage

As device operating bias increases, P and Q increase proportional to k_s until Q is of sufficient magnitude to sustain hole ionization feedback. Under these bias conditions, both P and Q are still quite low, so the carrier multiplication in each gain stage is low; hence, the device may be approximated by the two-carrier discrete-gain-stage model of Equation 9. As can be observed in Figure 8, the measured data can be approximated by Equation 9 (where k_s = 0.036). In this bias range, the measured 7-stage and 10-stage SCM APD data are well below the McIntyre model of Equation 4 (where k = 0.036) of a bulk semiconductor multiplication region APD with no dead space.

To gain insight into the carrier dynamics of an SCM APD, a band-edge modeler was used to estimate the electric field in each device as a function of bias. The estimated electric-field curves are plotted in Figure 9 with the electron ionization probabilities estimated by Equation 10 for the average gain

measured at each bias. For example, for a 7-stage device at gain of $M_{DC} = 42$, where the 7-stage data deviate from Equation 9 (where $k_s = 0.036$), carrier probabilities of $P = 0.47$ and $Q = 0.02$ can be calculated from Equation 10 (where $k_s = 0.036$). The same carrier ionization probabilities would result in a gain of: $M_{DC} \approx 9$ for a 5-stage device; and avalanche breakdown for a 10-stage SCM APD. Similarly, the data in Figure 9 show that, for any M_{DC}, a 10-stage device operates with a lower electric field than a 7-stage or 5-stage device. For example, for $M_{DC} = 42$, the electric field of the 10-stage SCM APD is 595 kV/cm; whereas the 7-stage and 5-stage devices are 636 kV/cm and 676 kV/cm, respectively. This is expected because less gain is needed in each stage due to the increased number of gain stages in the multiplication region.
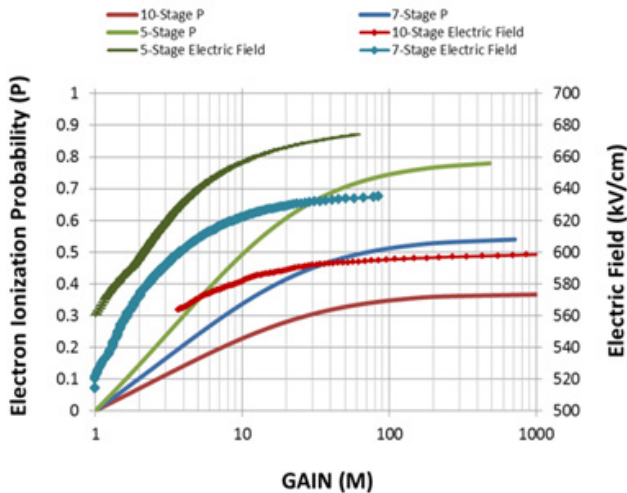
Figure 9: Probability of electron ionization per stage from Equation 7 (where $k_s = 0.036$), as a function of gain and the electric field estimated from the I-V curves using the band-edge modeler.

A lower electric field is important because it reduces the magnitude of the electric-field-dependent trap-assisted tunneling dark current. [45] The relationship between electric field and dark current generation in the various SCM APDs is illustrated in Figure 6. The I-V curves show that, at any M_{DC}, the 10-stage SCM APDs operate with lower dark current than the devices with fewer gain stages.

To elucidate the effects of the electric field on the multi-stage SCM APDs, the electric field and excess noise are plotted in Figure 10 as a function of output gain. For an excess noise of $F(M_{DC}) = 3$, Figure 10 shows that the 5-, 7-, and 10-stage devices are operated with electric fields of 670, 635, and 595 kV/cm, respectively; and, from Figure 9, it can be determined that operation under these electric fields results

in $P \approx 0.7$, 0.5, and 0.36, respectively. For each of the various numbered gain stages, the data illustrate the electric fields needed to achieve specific values of P and Q and to show the impact the SCM-APD design has on M_{DC} and $F(M_{DC})$.

The plots of Figure 11 help to illustrate further the interplay between the number of gain stages and the electric-field-dependent carrier ionization probabilities on the gain and excess noise resulting from ionization feedback.
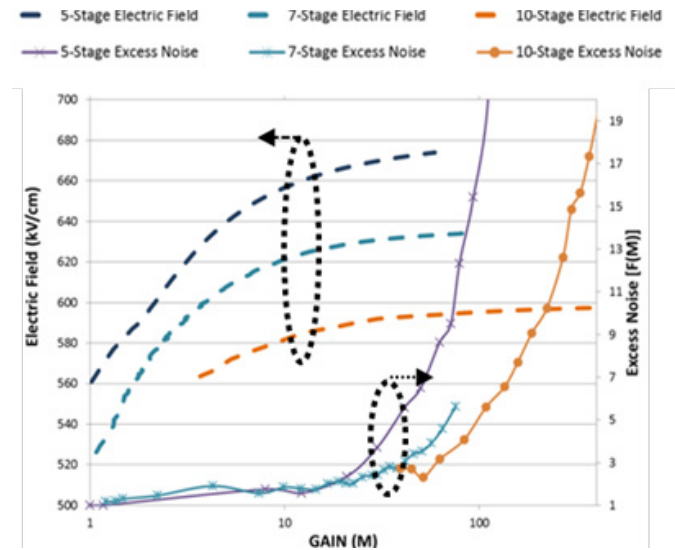
Figure 10: The electric field estimated by the band-edge modeler as a function of output gain level for the 5-stage, 7-stage, and 10-stage SCM-APD devices. Also plotted is the measured excess noise for each device.
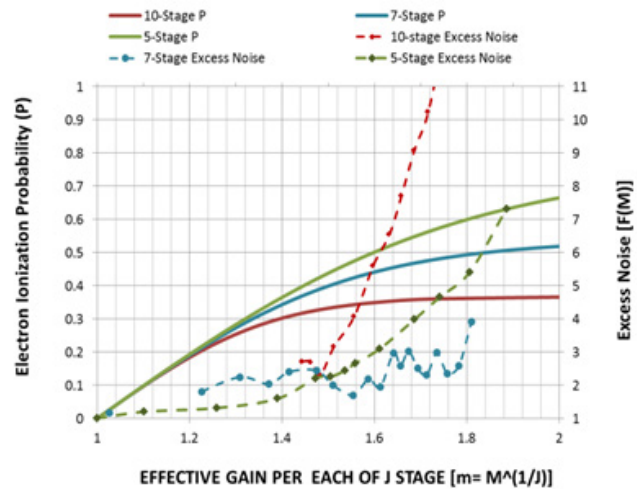
Figure 11: The measured excess noise and the electron ionization probability, P, calculated from Equation 10, plotted as a function of the effective gain per stage ($m_{eff} = \langle M_{DC} \rangle 1/J$).

[45] S. R. Forrest, "Performance of InxGa1-xAsyP1-yphotodiodes with dark current limited by diffusion, generation recombination, and tunnelling," IEEE J. Quantum Electron., vol. 17, pp. 217–226, Feb. 1981.

In Figure 11, the estimated electron ionization probabilities from Equation 10 for $k_s = 0.036$ and the measured excess noise values are plotted as a function of the average effective gain per stage, calculated assuming that all of the SCM-APD gain occurs without ionization feedback; the effective gain for each stage is calculated using $m_{eff} = M_{DC}1/J$. It is interesting to note that, in Figure 11, the excess noise data do not coincide with the incremented number of gain stages. For example, at $F(M_{DC}) = 3$, the 7-stage device operates at an effective gain per stage of approximately $m_{eff} = 1.8$, whereas the 5-stage device operates at $m_{eff} = 1.6$, and the 10-stage operates at $m_{eff} = 1.5$. This result illustrates the effect that carrier ionization probabilities (increased electric fields) and the number of gain stages have on the DC gain and excess noise. It also demonstrates that, as the number of gain stages increases, small increases in hole ionization feedback can significantly impact the gain and excess noise of the SCM APD.

Higher Gain Per Stage/Higher Feedback "Bulk-Like" Multiplication

When the bias is increased to higher output gain levels, P and Q continue to increase in proportion to one another and, with a sufficient number of gain stages to support ionization feedback, the excess noise models for bulk semiconductor multiplication regions (i.e., Equation 4) can be applied to the SCM APD. Only the 10-stage device has a sufficient number of gain stages for these conditions to apply. For the 10-stage SCM APDs, the measured data can be approximated by Equation 4 (where $k = 0.036$) above $M_{DC} \approx 125$. At this gain, Equation 10 (where $k_s = 0.036$) can be used to determine that $P = 0.35$. When Equation 10 (where $k_s = 0.036$) is used at this same electron ionization probability, the 5-stage and 7-stage devices have DC gains of $M_{DC} = 5.14$ and $M_{DC} = 11.58$, respectively.

Increased Multiplication Approaching Breakdown Due to Increased Hole Feedback

At even higher biases, the increased P and Q cause ionization feedback effects to dominate the excess noise performance as the device approaches avalanche breakdown. The 5-stage SCM APD deviates from Equation 9 (where $k_s = 0.036$), at $M_{DC} \approx 14$; and the 7-stage device deviates at $M_{DC} \approx 42$. at these output gain values, Equation 10 (where $k_s = 0.036$) can be used to calculate $P = 0.6$ for the 5-stage SCM APD and $P = 0.47$ for the 7-stage device.

Avalanche Breakdown

At higher biases, the 5-stage and 7-stage SCM APDs experience avalanche breakdown, whereas, the 10-stage SCM APDs do not. The lack of breakdown in the 10-stage devices is indicative of single-carrier-dominated (electron-dominated) ionization.

Performance Variability

The published literature lacks carrier impact-ionization rate data for the quaternary alloy $Al_{0.335}Ga_{0.140}In_{0.525}As$ over the range of electric fields and operating temperatures in which the SCM APD is operated. The lack of data prevents direct Monte Carlo or numeric modeling of temperature effects.

To test the effects of temperature and process variability on the performance of the SCM APD, 5-stage SCM APDs were tested over a range of temperatures. These data are plotted in Figure 12 alongside data for two 7-stage devices tested at 295 K and the 10-stage SCM-APD device tested at 185 K. All of the data show good approximation to Equation 9, $k_s = 0.036$, over the expected gain ranges, and the deviation of the 5-stage SMC-APD data from Equation 9, $k_s = 0.036$, at approximately $M_{DC} = 13$ ($P = 0.54$) is consistent between devices over the range of temperatures. While some measurement variability is present, the overlap of the various device performances at low gains indicates good calibration in the measurements.
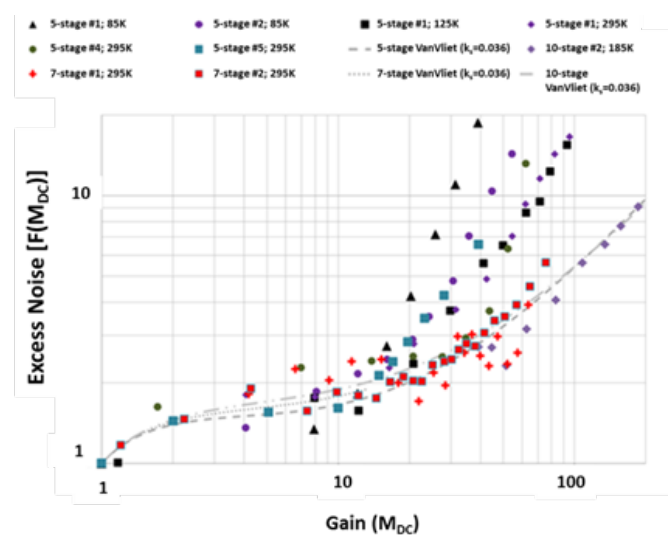

Figure 12: Plot of 5-stage SCM APDs measured at various temperatures, shown alongside the measured excess noise data from two 7-stage devices and a 10-stage device. Also shown for reference is Equation 9, $k_s = 0.036$, plotted for each of the number of gain stages.

There is some indication in the 5-stage SCM-APD data that, at lower temperatures, avalanche breakdown may occur at a faster rate than the higher operating temperatures. This may be a result of reduced photon scattering of holes in the "cool down" region of the gain stages (Figure 2, inset label iii) at low temperatures, leading to increased hole ionization feedback effects as bias is increased.

CONCLUSION

Multistage InGaAs/InAlAs SCM-APD designs were shown to operate at high linear-mode gain with low excess noise. The cascaded series of asymmetric multiplication stages in the SCM APDs employ variations of alloy composition, layer thickness, and doping to modulate carrier energy and associated dead space inside the junction, maximizing electron-initiated impact ionization while minimizing hole ionization.

The SCM-APD design has been analyzed using Monte Carlo and numerical simulations, which are in good agreement. The designs were empirically validated through growth,

fabrication, and test of multiple implementations. The performance of the devices was shown to be approximated by analytical models previously developed for discrete gain stage "staircase" and low ionization feedback "superlattice" APDs.

At equivalent output signal gains, the SCM APDs with more multiplication stages were shown to display less excess noise and less dark current than those devices with fewer gain stages. Select 10-stage devices exhibited gains exceeding 6,000, with excess noise characterized by $k < 0.04$ for $150 < M_{DC} < 1300$, and with sub-McIntyre performance (i.e., Equation 4, where $k = 0.036$) at gains up to approximately $M_{DC} = 125$.

This level of room-temperature gain with low excess noise exceeds that of the published results known for InGaAs and HgCdTe APDs, which makes the innovation promising for the range of scientific and communications applications that require compact, robust, linear, short-wave infrared (SWIR) photodetectors with high internal gain.

MCO-0001215
P0196

INNOVATION WITH PURPOSE

955 PERIMETER ROAD • MANCHESTER, NH 03103 • USA
+1-603-626-2300 • FAX: +1-603-641-5336 • ALLEGROMICRO.COM